Research Papers

GREENSUSMATER

Greensusmater
Vol. 2, No. 2, 2025
https://doi.org/10.62755/greensusmater.2025.2.2.30-35

Check for updates

Thermal Annealing Tailors Crystallinity and Magnetism in Silica-Coated Ni–Zn Ferrite (SiO_2@$NiZnFe_2O_4$) Nanoparticles

Januar Widakdo[1]

[1] *Department of Physics, Faculty of Mathematics and Natural Sciences, Universitas Indonesia, Depok 16424, Indonesia*

Corresponding author: januar.widakdo@ui.ac.id

ARTICLE HISTORY: Received: July 7, 2025 | Revised: September 12, 2025 | Accepted: September 18, 2025

ABSTRACT

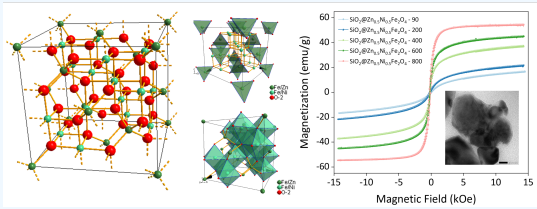

$Ni_{0.5}Zn_{0.5}Fe_2O_4$ nanoparticles were synthesized using a co-precipitation method followed by annealing at different temperatures to investigate their structural, morphological, and magnetic properties. X-ray diffraction (XRD) confirmed the formation of a single-phase spinel structure, with increased crystallinity and grain growth observed at higher annealing temperatures. Transmission electron microscopy (TEM) and selected area electron diffraction (SAED) further revealed a transition from small, aggregated nanoparticles to well-defined crystalline grains. Magnetic hysteresis measurements demonstrated a significant enhancement in saturation magnetization (Ms) and coercivity (Hc) with increasing temperature, reaching up to 55.15 emu/g and 253.23 Oe, respectively, at 800 °C. These improvements are attributed to reduced surface spin disorder and increased magnetic domain alignment due to grain growth. The results underscore the importance of annealing temperature in tailoring the magnetic behavior and structural properties of Ni–Zn ferrite nanoparticles for potential applications in magnetic and electronic devices.

Keywords: *Spinel ferrite; Nanoparticles; Magnetic properties; Annealing temperature; Ni–Zn ferrite*

1. INTRODUCTION

Magnetic nanoparticles have been extensively investigated over the past few decades due to their superparamagnetic behavior, high saturation magnetization, and favorable relaxation dynamics [1–3]. These characteristics make them highly suitable for various biomedical and technological applications, including magnetic resonance imaging (MRI) and hyperthermia therapy, drug and gene delivery, bioseparation, and quantitative immunoassays [4–6]. Among the most widely studied magnetic materials are Fe-based nanoparticles such as Fe_2O_3 [7] and Fe_3O_4 [8], as well as spinel ferrites such as $NiFe_2O_4$ [9, 10], $ZnFe_2O_4$ [11, 12], $MnFe_2O_4$ [13], and $CoFe_2O_4$ [14]. However, pure Fe-based metallic nanoparticles often suffer from chemical instability, prompting significant interest in more stable ferrite compounds with a spinel structure (AB_2O_4).

The magnetic behavior of spinel ferrites is largely governed by the nature of the metal cations occupying the tetrahedral (A) and octahedral (B) sites [15]. Tailoring the magnetic and chemical properties of ferrites through the incorporation of transition metals such as Ni, Zn, Mn, and Co has become a fundamental strategy for optimizing performance. Ni–Zn ferrites are considered highly versatile due to their low coercivity, high saturation magnetization, high Curie temperature, chemical stability, and biodegradability. These properties render them ideal candidates for biological and medical applications, provided the nanoparticles are monodispersed and compatible with biomolecular functionalization [16, 17].

The physical properties of Ni–Zn ferrites are critically dependent on factors such as chemical composition, particle size, sintering conditions, and synthesis method [18, 19]. Among the available synthesis approaches, wet chemical techniques such as microemulsion, hydrothermal-microwave, hydrothermal synthesis, and sol–gel methods have proven effective in producing nanoscale ferrite powders at reduced reaction temperatures. The co-precipitation method offers excellent control over stoichiometry and results in homogeneous, reproducible ferrite powders [20–22].

In this work, $Ni_{0.5}Zn_{0.5}Fe_2O_4$ nanoparticles were synthesized using a co-precipitation method and subjected to sintering at various temperatures to investigate the effect of thermal treatment on their structural and magnetic properties. To enhance dispersibility and biocompatibility, selected samples were further encapsulated with silica. Comprehensive characterization using X-ray diffraction (XRD), transmission electron microscopy (TEM), Fourier transform infrared spectroscopy (FTIR), and vibrating sample magnetometry (VSM) was carried out. The study aims to elucidate the relationship between annealing temperature, silica encapsulation, and the resulting microstructural and magnetic behavior of Ni–Zn ferrite nanoparticles for potential functional applications.

2. MATERIALS AND METHODS

2.1 Materials

The precursors used in this study include iron(III) chloride hexahydrate ($FeCl_3 \cdot 6H_2O$),zinc sulfate heptahydrate ($ZnSO_4 \cdot 7H_2O$),nickel(II) chloride hexahydrate ($NiCl_2 \cdot 6H_2O$),and sodium hydroxide (NaOH), all of analytical grade and purchased from Merck (Germany). Hydrochloric acid (HCl, 37%) was also obtained from Merck

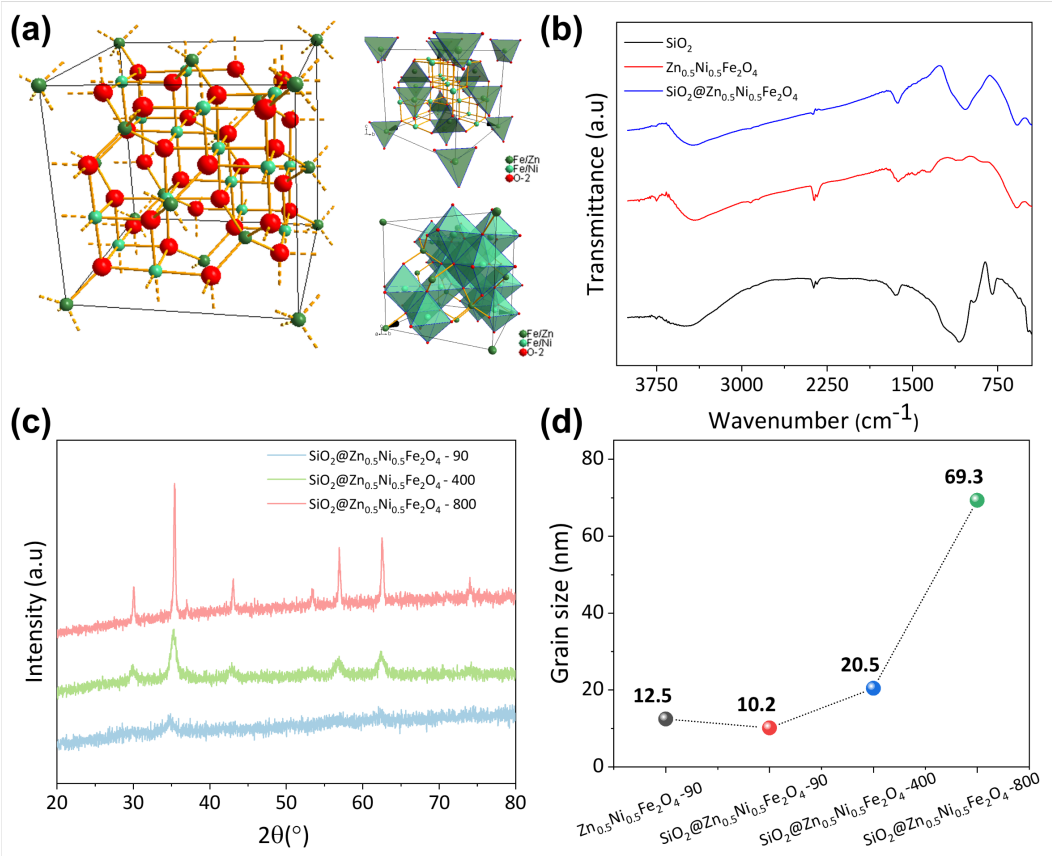

Figure 1. (a) Crystal structure of $Ni_{0.5}Zn_{0.5}Fe_2O_4$. (b) FTIR spectra of synthesized samples. (c) XRD patterns of samples annealed at various temperatures. (d) Grain size variation with annealing temperature and silica coating.

and used without further purification. Deionized water (aquadest) was used throughout the synthesis process.

2.2 Fabrication of $Ni_{0.5}Zn_{0.5}Fe_2O_4$ Nanoparticle

$Ni_{0.5}Zn_{0.5}Fe_2O_4$ nanoparticles were synthesized via co-precipitation. Stoichiometric amounts of $ZnSO_4 \cdot 7\,H_2O$ and $NiCl_2 \cdot 6\,H_2O$ were dissolved in 20 mL deionized water. Separately, $FeCl_3 \cdot 6\,H_2O$ and NaOH were each dissolved in 50 mL deionized water. The metal-salt solutions were combined, and 3.37 mL of concentrated HCl (37%) was added to assist homogenization and pH control. The mixed solution was introduced dropwise into 1.5 M NaOH under continuous stirring (1000 rpm) at 90 °C for 1 h to induce precipitation. The precipitate was washed with deionized water six times and dried at 90 °C for 5 h. For silica coating, 10 wt% SiO2 (relative to ferrite mass) was added to selected wet powders prior to heat treatment to obtain $SiO_2@Ni_{0.5}Zn_{0.5}Fe_2O_4$ composites. All powders (coated and, where applicable, uncoated controls) were subsequently annealed in air using a programmable muffle furnace with a heating rate of 5 °C min^{-1}, held at the target temperature for 2 h, and then furnace-cooled to room temperature. Samples are denoted $SiO_2@Ni_{0.5}Zn_{0.5}Fe_2O_4$-xxx, where xxx is the annealing temperature in °C (e.g., $SiO_2@Ni_{0.5}Zn_{0.5}Fe_2O_4$-200, -400, -600, and -800). Uncoated reference samples follow the analogous notation which named $SiO_2@Ni_{0.5}Zn_{0.5}Fe_2O_4$-90.

2.3 Materials Characterizations

The crystallographic structure of the samples was analyzed using X-ray diffraction (XRD, Shimadzu XD) equipped with Cu Kα_1 radiation (λ = 1.5406 Å). Magnetic properties were measured using a Vibrating Sample Magnetometer (VSM, Riken Denshi Co. Ltd.) under a maximum applied magnetic field of 15 kOe at room temperature. Morphological features were examined via Transmission Electron Microscopy (TEM, JEOL JEM-4000). Fourier Transform Infrared Spectroscopy (FTIR, Shimadzu Prestige-21) was employed to investigate the chemical bonding and functional groups present in the samples.

3. RESULTS AND DISCUSSION

3.1 Structural Morphology of $Ni_{0.5}Zn_{0.5}Fe_2O_4$ Nanoparticles

Figure 1a illustrates the spinel crystal structure of $Ni_{0.5}Zn_{0.5}Fe_2O_4$, in which metal cations occupy both tetrahedral (A) and octahedral (B) sites within a face-centered cubic lattice formed by oxygen anions. In this inverse spinel configuration, Ni^{2+} ions predominantly occupy octahedral sites, Zn^{2+} ions preferentially occupy tetrahedral sites, while Fe^{3+} ions are distributed over both. This specific distribution strongly affects the material's magnetic and structural properties, which are sensitive to annealing temperature and compositional adjustments. Figure 1b displays the FTIR spectra of SiO_2, $Ni_{0.5}Zn_{0.5}Fe_2O_4$ nanoparticles, and the silica-coated composite $SiO_2@Ni_{0.5}Zn_{0.5}Fe_2O_4$ over 3750–500 cm^{-1}. All spectra exhibit a broad envelope near 3400 cm^{-1} together with a band at ~1630–1650 cm^{-1}, attributable to O–H stretching and H–O–H bending of adsorbed/lattice water, respectively; a weak feature around 2350 cm^{-1}. The SiO_2 reference shows the characteristic Si–O–Si asymmetric stretching cen-

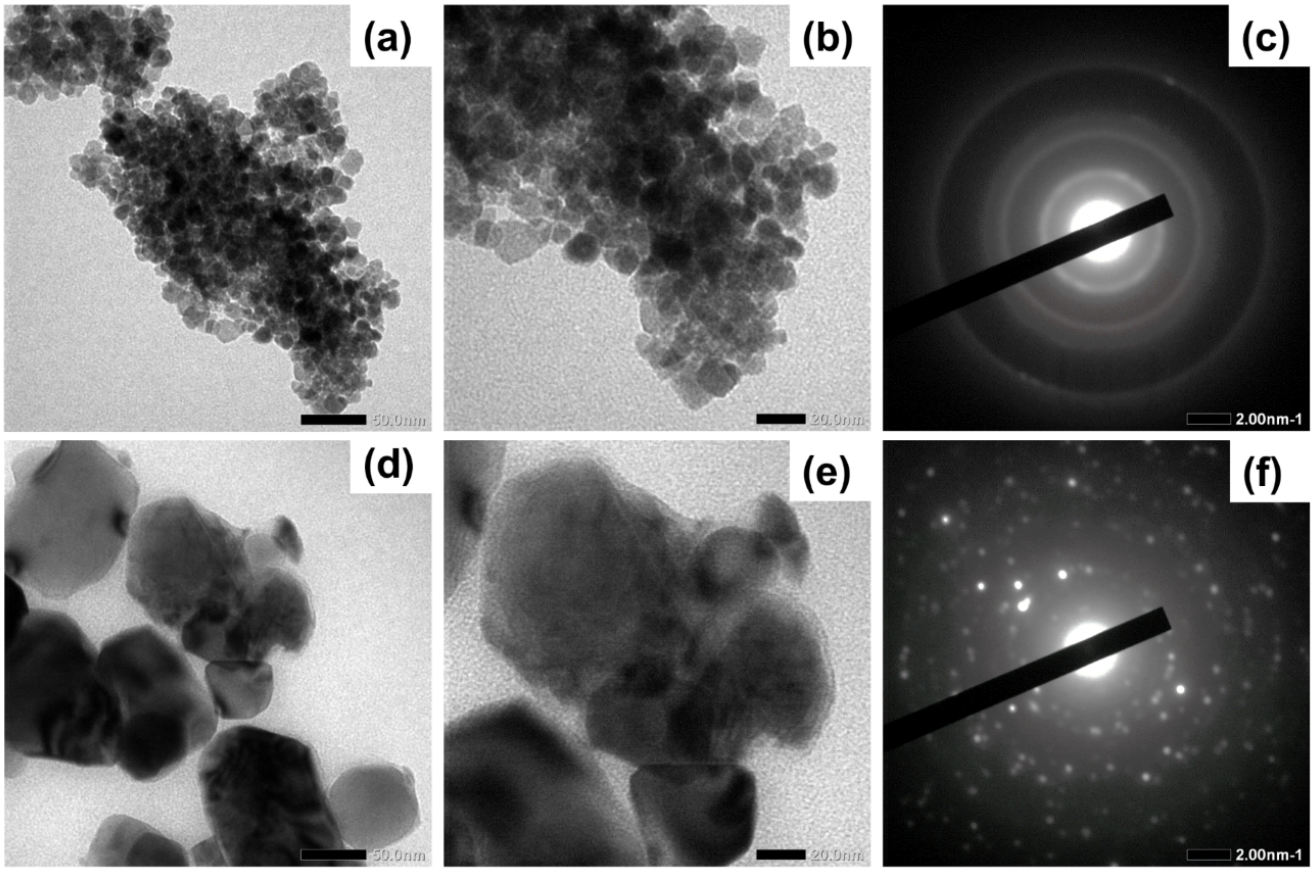

Figure 2. TEM and SAED images of SiO_2@$Ni_{0.5}Zn_{0.5}Fe_2O_4$-400 nanoparticles (a–c) and SiO_2@$Ni_{0.5}Zn_{0.5}Fe_2O_4$-800 (d–f). Low-temperature samples show small, aggregated particles with diffuse rings, while high-temperature samples exhibit larger grains with distinct diffraction spots.

tered at ~1080 cm^{-1}, accompanied by the symmetric stretching near ~800–850 cm^{-1} and the Si–O rocking mode below ~470 cm^{-1}, consistent with amorphous silica [23]. In contrast, the bare ferrite lacks the silica signatures at ~1080 and ~800 cm^{-1} and exhibits a low-frequency band emerging in the 550–600 cm^{-1} region, assignable to Fe–O stretching in the spinel lattice [24]. The spectrum of SiO_2@$Ni_{0.5}Zn_{0.5}Fe_2O_4$ combines these features: the pronounced ~1080 and ~800 cm^{-1} bands confirm the silica shell, while a weaker Fe–O band persists around ~560–590 cm^{-1}, indicating retention of the ferrite core. The slightly stronger O–H envelope in the coated sample is consistent with surface silanol (Si–OH) groups.

The XRD patterns of $Ni_{0.5}Zn_{0.5}Fe_2O_4$ nanoparticles annealed at 90°C, 400°C, and 800°C are shown in Figure 1c. The diffraction peaks are indexed to the cubic spinel structure of Ni–Zn ferrite, consistent with JCPDS card No. 08-0234, confirming phase purity even at the lowest annealing temperature. At 90°C (SiO_2@$Ni_{0.5}Zn_{0.5}Fe_2O_4$-90), the broad and weak peaks indicate poor crystallinity. As the annealing temperature increases, the diffraction peaks become sharper and more intense, suggesting improved crystallinity and grain growth. Crystallite size was estimated using the Scherrer equation from the full width at half maximum (FWHM) of the (311) peak. As shown in Figure 1d, the average crystallite size increases from approximately 14 nm at 400°C to about 45 nm at 800°C. The silica-coated samples annealed at lower temperatures maintain smaller grain sizes (10–13 nm), indicating that the presence of silica may inhibit grain growth during thermal treatment. These results emphasize that annealing temperature significantly influences the crystallinity and grain size of $Ni_{0.5}Zn_{0.5}Fe_2O_4$ nanoparticles, with higher temperatures promoting larger, well-crystallized structures.

The morphology and microstructure of SiO_2@$Ni_{0.5}Zn_{0.5}Fe_2O_4$-90 nanoparticles were examined using Transmission Electron Microscopy (TEM), with corresponding Selected Area Electron Diffraction (SAED) patterns, as shown in Figure 2. Figures 2a–c present the TEM and SAED results for the sample annealed at 400°C (SiO_2@$Ni_{0.5}Zn_{0.5}Fe_2O_4$-400). The images reveal highly agglomerated and uniformly distributed nanoparticles with near-spherical shapes and sizes in the nanometer range. The SAED pattern (Figure 2c) shows diffuse concentric rings, indicating the polycrystalline nature of the sample but with relatively poor crystallinity, consistent with the broad XRD peaks observed at this temperature.

In contrast, the nanoparticles annealed at 800°C (SiO_2@$Ni_{0.5}Zn_{0.5}Fe_2O_4$-800, Figures 2d–f) exhibit significant grain growth and coalescence. The particles become larger and more irregular in shape, with clearer grain boundaries. The corresponding SAED pattern (Figure 2f) displays distinct and sharp diffraction spots, confirming enhanced crystallinity and well-defined lattice planes at elevated annealing temperatures. These observations are in agreement with the XRD results and crystallite size analysis (Figure 1d), further supporting the role of thermal treatment in promoting crystal growth and structural order. Overall, the TEM and SAED

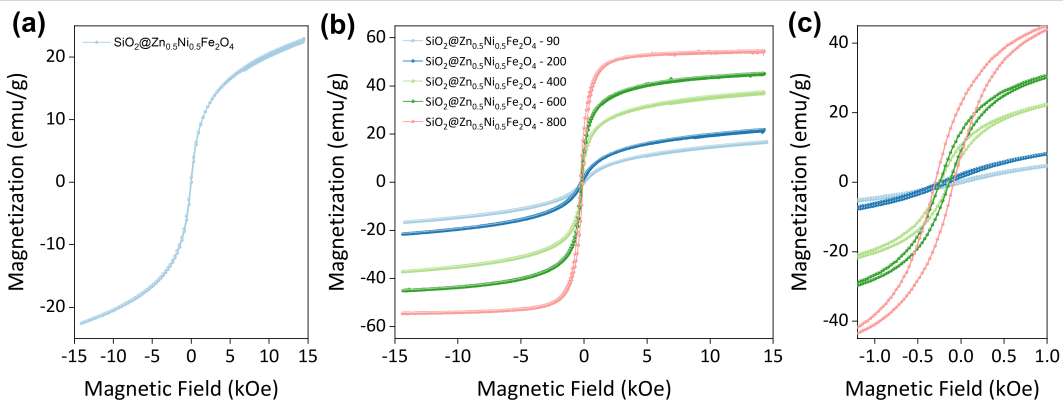

Figure 3. Magnetic hysteresis loops at room temperature. (a) Representative loop of SiO_2@$Ni_{0.5}Zn_{0.5}Fe_2O_4$. (b) SiO_2@$Ni_{0.5}Zn_{0.5}Fe_2O_4$ annealed at 90, 200, 400, 600, and 800 °C. (c) Low-field magnification of (b) highlighting the increase in saturation magnetization, remanence, and coercivity with annealing.

analyses demonstrate that annealing temperature strongly influences both particle morphology and crystallinity. Lower temperatures yield small, poorly crystallized particles, while higher temperatures promote larger, well-ordered grains with higher structural coherence.

The TEM/SAED evolution from agglomerated nano crystallites at 400°C (diffuse rings) to faceted, well-defined grains at 800°C (spotty pattern) reflects thermally driven coarsening that minimizes total interfacial energy [25]. As temperature rises, desorption of adsorbed water and residual ligands reduces electrostatic/steric barriers between primary particles, enabling particle–particle contact and neck formation. Enhanced surface and grain-boundary diffusion then promote sintering/coalescence and occasional oriented attachment of crystallites with low misorientation [26]. In parallel, Ostwald ripening operates high-curvature (smaller) particles, which possess higher chemical potential, partially dissolve and redeposit onto larger ones, advancing grain boundary migration and growth [27]. The 5 °C min^{-1} ramp and 2 h hold provide sufficient diffusion time for these processes, converting loosely aggregated nanoparticles into larger, less defective crystallites with clearer lattice order—consistent with the transition from diffuse rings to discrete diffraction spots in SAED and with the improved crystallinity inferred from XRD.

3.2 Magnetic Properties of $Ni_{0.5}Zn_{0.5}Fe_2O_4$ Nanoparticles

The magnetic behavior of Ni0.5Zn0.5Fe2O4 nanoparticles was investigated using vibrating sample magnetometry (VSM) at room temperature, as shown in Figure 3 and summarized in Table 1. The magnetic hysteresis loop of the as-prepared (non-annealed) $Ni_0 \cdot 5\,Zn_0 \cdot 5\,Fe_2O_4$ sample (Figure 3a) displays a narrow loop with a low saturation magnetization (Ms) of 22.93 emu/g, suggesting the presence of a soft magnetic nature with superparamagnetic tendencies due to its small crystallinity and poor crystallinity. Figure 3b and 3c reveal the evolution of the magnetic hysteresis loops as a function of annealing temperature. A noticeable enhancement in magnetic performance is observed with increasing annealing temperature. The Ms values increased significantly from 16.87 emu/g at 90°C to 55.15 emu/g at 800°C. This increase is attributed to improved crystallinity, reduction in surface spin disorder, and grain growth, as previously evidenced by XRD and TEM results.

Similarly, remanent magnetization (Mr) and coercivity (Hc) also exhibit upward trends with increasing temperature. Mr increases from 0.29 emu/g (90°C) to 14.57 emu/g (SiO_2@$Ni_{0.5}Zn_{0.5}Fe_2O_4$-800), while Hc increases from 45.22 Oe to 253.23 Oe. These changes indicate a transition from superparamagnetic behavior at low temperatures toward ferrimagnetic behavior at higher temperatures, likely due to enhanced magnetic domain alignment and reduced surface effects in larger crystallites. The squareness ratio (Mr/Ms), which provides insights into the magnetic domain state, also increases with annealing temperature, from 0.017 at 90°C to 0.264 at 800°C. This suggests a shift toward multi-domain particle behavior and more stable magnetic configurations at higher temperatures. Overall, the data confirm that thermal treatment plays a critical role in modulating the magnetic properties of SiO_2@$Ni_{0.5}Zn_{0.5}Fe_2O_4$-90 nanoparticles. Higher annealing temperatures lead to increased magnetic ordering, improved crystallinity, and larger grain sizes, which collectively enhance the material's magnetic performance.

With increasing annealing temperature, the hysteresis loops in Figure 3b (low-field zoom in Figure 3c) evolves from narrow, S-shaped curves into wider, squarer loops with higher saturation, reflecting three coupled mechanisms. First, annealing heals structural defects and relaxes strain at surfaces and grain boundaries [28], while driving cation redistribution toward the equilibrium spinel configuration (Zn^{2+} → A sites, Ni^{2+} → B sites); both effects restore A–B super exchange and align previously canted surface spins, yielding a higher net moment Ms [28]. Second, grain growth increases the particle volume and reduces the surface-to-volume ratio, diminishing the fraction of disordered "dead-layer" spins and thereby raising both Ms and the remanence Mr [29].

These annealing-driven improvements map directly onto common device needs. Higher crystallinity and grain size yield larger Ms and blocked behavior at room temperature, enabling efficient magnetic capture/actuation of particulate systems (e.g., magnetically recoverable adsorbents/catalysts) and stronger signals in magnetic sensing. For RF/EMI uses, the more ordered Ni–Zn ferrite produced at 400–800°C offers higher permeability while retaining the intrinsically high resistivity of Ni–Zn ferrites, which helps limit eddy-current loss—relevant to inductor cores, EMI-suppression beads, and microwave absorbers. Conversely, lower-temperature samples with smaller grains and lower Hc approach superparamagnetic response, advantageous where rapid "on/off" mag-

Table 1. Magnetic parameters of $Ni_{0.5}Zn_{0.5}Fe_2O_4$ nanoparticles annealed at various temperatures, including saturation magnetization (M_s), remanent magnetization (M_r), coercivity (H_c), and squareness ratio (M_r/M_s).

Nanoparticle	M_s (emu/g)	M_r (emu/g)	H_c (Oe)	M_r/M_s
$Ni_{0.5}Zn_{0.5}Fe_2O_4$	22.93	0.59	48.03	0.03
SiO_2@$Ni_{0.5}Zn_{0.5}Fe_2O_4$-90	16.87	0.29	45.22	0.02
SiO_2@$Ni_{0.5}Zn_{0.5}Fe_2O_4$-200	21.85	1.84	198.01	0.08
SiO_2@$Ni_{0.5}Zn_{0.5}Fe_2O_4$-400	37.52	8.46	249.30	0.23
SiO_2@$Ni_{0.5}Zn_{0.5}Fe_2O_4$-600	45.68	11.23	236.10	0.25
SiO_2@$Ni_{0.5}Zn_{0.5}Fe_2O_4$-800	55.15	14.57	253.23	0.27

netization is required (e.g., magnetic separation or targeting when appropriately surface-passivated). Thus, tuning annealing temperature provides a practical handle to select magnetic performance for specific application windows [30–32].

4. CONCLUSION

$Ni_{0.5}Zn_{0.5}Fe_2O_4$ nanoparticles were successfully synthesized via a co-precipitation method and annealed at various temperatures to study the effects on their structural, morphological, and magnetic properties. XRD analysis confirmed the formation of a single-phase spinel structure at all temperatures, with crystallinity and grain size increasing significantly at higher annealing temperatures. TEM and SAED observations supported these findings, showing a transition from small, agglomerated particles at low temperature to well-defined grains at 800°C. Magnetic characterization revealed that both saturation magnetization and coercivity improved with annealing, reaching maximum values of 55.15 emu/g and 253.23 Oe, respectively, at 800°C. These enhancements are attributed to improved crystallinity, reduced surface spin disorder, and increased particle size. The study highlights the critical role of thermal treatment in tuning the magnetic and structural properties of $Ni_0 \cdot 5\,Zn_0 \cdot 5\,Fe_2O_4$, indicating its potential for applications in magnetic devices and nanotechnology.

DATA AVAILABILITY STATEMENT

The datasets generated during and/or analyzed during the current study are available from the corresponding author on reasonable request.

CONFLICT OF INTEREST

The authors declare that there are no conflicts of interest.

ACKNOWLEDGMENTS

This work was supported by Hibah Publikasi Terindeks Internasional (PUTI) Q1 Tahun Anggaran 2024-2025 (NKB-413/UN2.RST/HKP.05.00/2024).

REFERENCES

[1] J. Mohapatra, P. Joshi, J. Ping Liu, Low-dimensional hard magnetic materials, Progress in Materials Science 138 (2023) 101143. https://doi.org/10.1016/j.pmatsci.2023.101143.

[2] M. Hossain, B. Qin, B. Li, X. Duan, Synthesis, characterization, properties and applications of two-dimensional magnetic materials, Nano Today 42 (2022) 101338. https://doi.org/10.1016/j.nantod.2021.101338.

[3] J. He, H. Yuan, M. Nie, H. Guo, H. Yu, Z. Liu, R. Sun, Soft magnetic materials for power inductors: State of art and future development, Materials Today Electronics 6 (2023) 100066. https://doi.org/10.1016/j.mtelec.2023.100066.

[4] X. Wei, M.-L. Jin, H. Yang, X.-X. Wang, Y.-Z. Long, Z. Chen, Advances in 3D printing of magnetic materials: Fabrication, properties, and their applications, Journal of Advanced Ceramics 11 (5) (2022) 665–701. https://doi.org/10.1007/s40145-022-0567-5.

[5] C. Zhang, X. Li, L. Jiang, D. Tang, H. Xu, P. Zhao, J. Fu, Q. Zhou, Y. Chen, 3D Printing of Functional Magnetic Materials: From Design to Applications, Advanced Functional Materials 31 (34) (2021) 2102777. https://doi.org/10.1002/adfm.202102777.

[6] E. Elahi, M. A. Khan, M. Suleman, A. Dahshan, S. Rehman, H. Waseem Khalil, M. A. Rehman, A. M. Hassan, G. Koyyada, J. H. Kim, M. F. Khan, Recent innovations in 2D magnetic materials and their potential applications in the modern era, Materials Today 72 (2024) 183–206. https://doi.org/10.1016/j.mattod.2023.11.008.

[7] E. Puspitasari, M. Ginting, R. Ramlan, Preparation and Characterization of Fe2O3 from Iron Sand of the Coastal Sea of Cidaun Beach-South Cianjur (Indonesia) using the Co-precipitation Method, Science and Technology Indonesia 8 (4) (2023) 594–598. https://doi.org/10.26554/sti.2023.8.4.594-598.

[8] S. Liu, B. Yu, S. Wang, Y. Shen, H. Cong, Preparation, surface functionalization and application of Fe3O4 magnetic nanoparticles, Advances in Colloid and Interface Science 281 (2020) 102165. https://doi.org/10.1016/j.cis.2020.102165.

[9] S. K. Sushant, N. J. Choudhari, S. Patil, M. K. Rendale, S. N. Mathad, A. T. Pathan, Development of M–NiFe2O4 (Co, Mg, Cu, Zn, and Rare Earth Materials) and the Recent Major Applications, International Journal of Self-Propagating High-Temperature Synthesis 32 (2) (2023) 61–116. https://doi.org/10.3103/S1061386223020061.

[10] K. Bouferrache, Z. Charifi, H. Baaziz, A. M. Alsaad, A. Telfah, Electronic structure, magnetic and optic properties of spinel compound $NiFe_2O_4$, Semiconductor Science and Technology 35 (9) (2020) 095013. https://doi.org/10.1088/1361-6641/ab9845.

[11] F. Tabesh, S. Mallakpour, C. M. Hussain, Recent advances in magnetic semiconductor ZnFe2O4 nanoceramics: History, properties, synthesis, characterization, and applications, Journal of Solid State Chemistry 322 (2023) 123940. https://doi.org/10.1016/j.jssc.2023.123940.

[12] S. M. Hoque, M. S. Hossain, S. Choudhury, S. Akhter, F. Hyder, Synthesis and characterization of ZnFe2O4 nanoparticles and its biomedical applications, Materials Letters 162 (2016) 60–63. https://doi.org/10.1016/j.matlet.2015.09.066.

[13] T. D. H. Nguyen, M.-F. Lin, W.-D. Hsu, Investigations on electronic, magnetic, and optical properties of MnFe2O4 through first-principles calculations, Computational Materials Science 235 (2024) 112831. https://doi.org/10.1016/j.commatsci.2024.112831.

[14] F. Sharifianjazi, M. Moradi, N. Parvin, A. Nemati, A. Jafari Rad, N. Sheysi, A. Abouchenari, A. Mohammadi, S. Karbasi, Z. Ahmadi, A. Esmaeilkhanian, M. Irani, A. Pakseresht, S. Sahmani, M. Shahedi Asl, Magnetic CoFe2O4 nanoparticles doped with metal ions: A review, Ceramics International 46 (11) (2020) 18391–18412. https://doi.org/10.1016/j.ceramint.2020.04.202.

[15] M. Amiri, M. Salavati-Niasari, A. Akbari, Magnetic nanocar-

riers: Evolution of spinel ferrites for medical applications, Advances in Colloid and Interface Science 265 (2019) 29–44. https://doi.org/10.1016/j.cis.2019.01.003.

[16] J. Widakdo, N. Istikhomah, A. Rifianto, E. Suharyadi, T. Kato, S. Iwata, Crystal structures and magnetic properties of silica and polyethylene glycol (PEG-4000) — Encapsulated Zn0.5Ni0.5Fe2O4 magnetic nanoparticles, in: 2017 IEEE 12th Nanotechnology Materials and Devices Conference (NMDC), IEEE, Singapore, 2017, pp. 149–150. https://doi.org/10.1109/NMDC.2017.8350535.
URL https://ieeexplore.ieee.org/document/8350535/

[17] N. Istikhomah, J. Widakdo, A. Rifianto, E. Suharyadi, T. Kato, S. Iwata, Effect of Zn concentration on crystal structure and magnetic properties of $Zn_xNi_{1-x}Fe_2O_4$ nanoparticles fabricated by co-precipitation method, in: 2017 IEEE 12th Nanotechnology Materials and Devices Conference (NMDC), IEEE, Singapore, 2017, pp. 151–152. https://doi.org/10.1109/NMDC.2017.8350536.
URL https://ieeexplore.ieee.org/document/8350536/

[18] A. Lakshmanan, P. Surendran, S. Sakthy Priya, K. Balakrishnan, P. Geetha, P. Rameshkumar, T. A. Hegde, G. Vinitha, K. Kannan, Investigations on structural, optical, dielectric, electronic polarizability, Z-scan and antibacterial properties of Ni/Zn/Fe2O4 nanoparticles fabricated by microwave-assisted combustion method, Journal of Photochemistry and Photobiology A: Chemistry 402 (2020) 112794. https://doi.org/10.1016/j.jphotochem.2020.112794.

[19] M. Xia, Y. Zhang, J. Xiao, P. Zhao, Z. Hou, F. Du, D. Chen, S. Dou, Magnetic field induced synthesis of (Ni, Zn)Fe2O4 spinel nanorod for enhanced alkaline hydrogen evolution reaction, Progress in Natural Science: Materials International 33 (2) (2023) 172–177. https://doi.org/10.1016/j.pnsc.2023.04.001.

[20] K. V. Chandekar, S. Yadav, Comprehensive study of MFe2O4 (M=Co, Ni, Zn) nanostructures prepared by co-precipitation route, Journal of Alloys and Compounds 960 (2023) 170838. https://doi.org/10.1016/j.jallcom.2023.170838.

[21] M. Rashad, E. Elsayed, M. Moharam, R. Abou-Shahba, A. Saba, Structure and magnetic properties of $Ni_xZn_{1-x}Fe_2O_4$ nanoparticles prepared through co-precipitation method, Journal of Alloys and Compounds 486 (1-2) (2009) 759–767. https://doi.org/10.1016/j.jallcom.2009.07.051.

[22] Y. Yi, Y. Peng, C. Xia, H. Deng, Y. Xiang, Q. Xia, Effects of heat treatment on structure and magnetic properties of Fe/(NiZn)Fe2O4 soft magnetic composite powders prepared using a co-precipitation method, Journal of Alloys and Compounds 728 (2017) 571–577. https://doi.org/10.1016/j.jallcom.2017.08.291.

[23] S. Alomairy, M. Al-Buriahi, E. Abdel Wahab, C. Sriwunkum, K. Shaaban, Synthesis, FTIR, and neutron/charged particle transmission properties of Pb3O4–SiO2–ZnO–WO3 glass system, Ceramics International 47 (12) (2021) 17322–17330. https://doi.org/10.1016/j.ceramint.2021.03.045.

[24] P. More, S. Kadam, P. Lokhande, G. Jangam, S. Patange, D. Satpute, Effect of sintering temperature on the structural, morphological, and the magnetic properties of Ni0.25Cu0.55 Zn0.20 Fe2O4 nano ferrite, Journal of Magnetism and Magnetic Materials 586 (2023) 171192. https://doi.org/10.1016/j.jmmm.2023.171192.

[25] S. Kumar, P. Pandey, K. Chattopadhyay, Influence of interfacial and strain energies on γ' coarsening kinetics in complex concentrated alloys, Materialia 33 (2024) 102018. https://doi.org/10.1016/j.mtla.2024.102018.

[26] F. Wakai, K. Brakke, Mechanics of sintering for coupled grain boundary and surface diffusion, Acta Materialia 59 (14) (2011) 5379–5387. https://doi.org/10.1016/j.actamat.2011.05.006.

[27] Y. Dong, D. Zhang, D. Li, H. Jia, W. Qin, Control of Ostwald ripening, Science China Materials 66 (3) (2023) 1249–1255. https://doi.org/10.1007/s40843-022-2233-3.

[28] J. Gubicza, Annealing-Induced Hardening in Ultrafine-Grained and Nanocrystalline Materials, Advanced Engineering Materials 22 (1) (2020) 1900507. https://doi.org/10.1002/adem.201900507.

[29] A. D Souza, P. Babu, S. Rayaprol, M. Murari, L. D. Mendonca, M. Daivajna, Size control on the magnetism of La0.7Sr0.3MnO3, Journal of Alloys and Compounds 797 (2019) 874–882. https://doi.org/10.1016/j.jallcom.2019.05.004.

[30] N. Maji, H. S. Dosanjh, Ferrite Nanoparticles as Catalysts in Organic Reactions: A Mini Review, Magnetochemistry 9 (6) (2023) 156. https://doi.org/10.3390/magnetochemistry9060156.

[31] M. F. Elmahaishi, R. S. Azis, I. Ismail, F. D. Muhammad, A review on electromagnetic microwave absorption properties: their materials and performance, Journal of Materials Research and Technology 20 (2022) 2188–2220. https://doi.org/10.1016/j.jmrt.2022.07.140.

[32] Y. Ha, S. Ko, I. Kim, Y. Huang, K. Mohanty, C. Huh, J. A. Maynard, Recent Advances Incorporating Superparamagnetic Nanoparticles into Immunoassays, ACS Applied Nano Materials 1 (2) (2018) 512–521. https://doi.org/10.1021/acsanm.7b00025.

